Size Dependent Optical Properties of Spherical $ZnO@Cu$ and $ZnO@Au$ Core/Shell Nanostructures

By

Tesfahun Gizat

A GRADUATE THESIS SUBMITTED TO
THE GRADUATE PROGRAM IN PARTIAL FULFILLMENT OF
THE REQUIREMENTS FOR THE DEGREE OF
MASTER OF SCIENCE IN PHYSICS AT
ADDIS ABABA UNIVERSITY

ADDIS ABABA, ETHIOPIA
FEBRUARY 2022

ADDIS ABABA UNIVERSITY
DEPARTMENT OF PHYSICS

The undersigned hereby certify that they have read and recommended to the Graduate Program of Addis Ababa University for acceptance a graduate thesis entitled "**Size Dependent Optical Properties of Spherical $ZnO@Cu$ and $ZnO@Au$ Core/Shell Nanostructures**" by **Tesfahun Gizat** in partial fulfillment of the requirements for the degree of **Master of Science** in Physics.

Dated: February 2022

Examiners: _____

_____

Supervisor: _____
Dr. Belayneh Mesfin

ADDIS ABABA UNIVERSITY

Date: **February 2022**

Author: **Tesfahun Gizat**

Title: **Size Dependent Optical Properties of Spherical $ZnO@Cu$ and $ZnO@Au$ Core/Shell Nanostructures**

Department: **Physics**

Degree: **M.Sc.** Convocation: **February** Year: **2022**

Permission is herewith granted to Addis Ababa University to circulate and to have copied for non-commercial purposes, at its discretion, the above title upon the request of individuals or institutions.

Signature of Author

DECLARATION

I, the undersigned, certify that all material in this M.Sc. thesis which is not my own work has been identified and duly acknowledged, and that no material has previously been submitted and approved for the award of a degree by this or any other university.

Author: _____
Tesfahun Gizat

This M.Sc. thesis has been submitted for examination with my approval as University research supervisor.

Supervisor: _____
Dr. Belayneh Mesfin

Place: **Department of Physics, Addis Ababa University**

Date: **February, 2022**

Table of Contents

List of Figures

Abstract

In this work, we studies the effect of size and thickness variation on the optical properties of a system that consists of spherical $ZnO@Cu$ and $ZnO@Au$ core-shell composite nanostructures embedded in a dielectric host matrix. The effective dielectric function, refractive index, and absorbance of the composite nanostructures are determined using the Maxwell-Garnett effective medium theory within the framework of the electrostatic approximation. The numerical simulation using nanoinclusions of radii 30 nm shows interesting behavior in the optical responses of the ensemble. In particular, it is shown that for different values of volume fraction and filling factor the refractive index and optical absorbance of the ensemble exhibited two sets of resonance peaks; the first set located around 515 nm and 490 nm and the second set found above 635 nm and 605 nm spectral regions for a system of $ZnO@Cu$ and $ZnO@Au$ nanoparticles, respectively. These peaks are attributed to the surface plasmon resonance of copper and gold at the core@metal and metal@host-matrix interface. Moreover, when the Cu and Au shell thickness is increased, the observed resonance peaks are enhanced; accompanied with slight red shifts for the first set of peaks and a blue shifts for the second set of peaks. In brief, it is seen that the optical properties of spherical $ZnO@Cu$ and $ZnO@Au$ core-shell nanoinclusions embedded in vacuum can be tuned by varying the shell thickness, filling factor, and/or volume fraction of the nanocomposites. The results obtained may be used in various applications such as sensors and nano-optoelectronics devices in optimizing material parameters to the desired values.

Acknowledgements

First and for most I would like to express my gratitude to my advisor Dr. Belayneh Mesfin for his invaluable assistance, support, and guidance. This work has never been materialized without the help of my advisor. My thanks goes also to the department of physics of Addis Ababa University (AAU) for their lovely help and motivation in my work. I also thank for their valuable attention and constructive comments and suggestions during presentation. I would also like to thank Kebridhar University for its sponsorship to attend this Masters degree program at Addis Ababa University. Furthermore, my thanks goes also to my friends and classmates for their support, encouragement, and helpful discussion in AAU. Last but not least, I want to express my love and gratitude to my beloved wife Habtam Mesganew and my daughter Yabsira for their understanding, support, and love through the duration of my studies.

Tesfahun Gizat
Addis Ababa, Ethiopia
March, 2022

Chapter 1

Introduction

Core-shell nanostructures are a combination of two or more different materials such that multiple properties can be engineered. They are a subset of nanocomposite materials wherein these materials consists of a nanoparticle surrounded by a shell designated as core@shell nanostructures [1]. These nanomaterials have attracting increasing research interests due to their unique structural characteristics that are not present in either the core or the shell but are possible only core-shell nanostructure exist [1, 2]. The purpose of these structures the possibility of combining different properties of varied materials [2]. Different types of core-shell nanostructures can be designated with a variety of combination of properties in mind such as dielectric-metal, dielectric-semiconductor, metal-dielectric and many others [1].

Most of the spherical nanoparticle are fabricated from noble metals such as silver (Ag), gold (Au), copper (Cu) and semiconductor (ZnO) materials are a few examples of such composite nanoparticles. They can display exceptional physical and chemical properties than the individual properties, which found a wide range of applications in nanotechnology [3].

There are different shapes of core-shell nanoparticles passed on the composite techniques. New techniques make it possible to prepare a variety of shapes not only spherical core-shell but nanostructures such as spherical, cylindrical, cube, hexagon

and tube. These shapes have also attracted the attention of researchers because of their different novel properties. The most common structures of core-shell nanoparticles are spherical when the spherical core is completely coated by shell nanoparticles [4].

With the development of nanoscience and nanotechnology mainly researches focus on the core-shell nanostructures. One motivation of using core-shell nanostructures is to achieve multiple functions. Another important motivation of utilizing core-shell nanostructure is to improve the properties as well as to reduce or diminish the drawback of nanoparticles. There are two directions in enhancing luminescence properties of nanoparticles: inhibit the negative factors and promote the positive factors [5].

The overall aim of this thesis is to investigation of size dependent optical properties of systems consisting of spherical core-shell $ZnO@Cu$ and $ZnO@Au$ nanostructures embedded in a dielectric host matrix. The core size and the thickness of the metallic shell are varied, simultaneously.

The paper is organized as follows: Chapter 1 describe the introductory part of the thesis. In Chapter 2, literature review, including CSNs, quantum effect and band gap, density of states and plasmonic properties are discussed. Chapter 3 deals with the modeling of spherical core-shell nanostructures. In Chapter 4 results and discussion related to complex refractive index and optical absorbance are presented. Finally, Chapter 5 displays the conclusion.

Chapter 2

Literature Review

Nanosized particles of core-shell materials have gained much more interests in recent year due to their desirable properties and applications in different areas such as catalysis, sensors, photo-electron devices, highly functional and effective device. These nanomaterials have novel electrical, structural, thermal, band gap engineering, plasmonic, tunability of nanostructures, and optical properties which are of high scientific interests in basic and applied fields. The confinement of particles in low dimensional structures leads to a fascinating change in their behavior and to the manifestation of novel size dependent effect which usually fall into the category of quantum size effect. Nanostructures are low dimensional structures.

2.1 Core-shell nanostructures

Core-shell nanostructures are made up of a combination of two or more different materials such that multiple properties can be engineered. They are a subset of nanocomposite materials wherein these materials consists of a nanoparticle surrounded by a shell designated as core-shell nanostructures [1]. These nanomaterials have attracted increasing research interests due to their unique properties that are not present in either the core or the shell but are possible only core-shell nanostructure exist [1, 2]. The purpose of these structures is the possibility of combining different properties of

varied materials. Thus, the physical properties of the core (ZnO) and shell (Cu and Au) are significantly altered. [1, 2]. By varying the chemical composition of the surface enhanced stability, higher surface area and optical properties can be achieved [1]. Comparatively, core-shell nanostructures have exhibited improved physical and chemical properties relative to their single component counterparts. The inherent emergent physical and chemical properties of the core-shell nanostructures are very important to the broader range of application, such as optics, electronics, catalysis and so forth [2]. Different types of core-shell nanostructures can be designated with a variety of combination of properties in mind such as dielectric-metal, dielectric-semiconductor, metal-dielectric, semiconductor-metal, and many others [1].

Combining different novel materials materials in a single nanocomposite gain much attentions due to the additional functionalities exhibited. Most is the spherical nanocomposites are designed from noble metals such as silver (Ag), gold (Au), copper (Cu) and semiconductor (ZnO) materials are a few examples of such composite nanoparticles. They can display exceptional physical and chemical properties than the individual particles, which found a wide range of applications in nanotechnology [3].

There are different shapes of core-shell nanoparticles passed on the composite techniques. New techniques make it possible to prepare a variety of shapes not only spherical core-shell but nanostructures such as cube, hexagon, and tube. These shapes have also attracted the attention of researchers because of their different novel properties. The most common structures of core-shell nanoparticles are spherical when the spherical core is completely coated by shell nanoparticles [4].

With the development of nanoscience and nanotechnology more and more researches focus on the core-shell nanostructures. One motivation of using core-shell nanostructures is to achieve multiple functions. Another important motivation of utilizing core-shell nanostructure is to improve the properties of nanoparticles. There

are two directions in enhancing luminescence properties of nanoparticles: inhibit the negative factors and promote the positive factors [5].

As stated in above, core-shell quantum dots are nearly earth like structures with its many layers and a core. Core is the basis of the quantum dot, controls the overall properties of the quantum dot as well as filters the light that shines through the quantum dots. Some of the most commonly used cores is ZnO, which have varying properties that make them more desirable to use than other materials. Zinc oxide (ZnO) quantum dots are efficient and have a high quantum dot yield. Quantum yield is the measure of the efficiency of photon emission as defined by the ratio of photons emitted to the number of photons absorbed [6]. ZnO nanostructures (NSs) are very attractive semiconductor for different photocatalysis processes because it possesses unique optical and electrical properties. ZnO is a wide band gap 3.37 eV compound semiconductor that is suitable for short wavelength optoelectronic applications. The high exciton binding energy (60 meV) in ZnO crystals can ensure excitonic emission at room temperature [7]. As a direct and wide band gap material ZnO has many advantage: higher breakdown voltage, ability to sustain large electric noise, high temperature, and higher operation. It is also stable under UV exposure. There exist various form of ZnO nanostructures such as nanoparticle, nanowires, nanorods, nanobelts, and nanotubs. It is easy to tune the ZnO NSs properties by controlling their size and morphology [8]. ZnO possesses emission/absorption bands in the wavelength ranges of the UV and visible lights. More attractively, ZnO is a promising candidate for the environmentally friendly nature and bio-compatibility in the medical systems. Consequently, there is considerable interest in studying ZnO in the form of powders, single crystals, thin films, or nanostructures [9, 10].

Even so, ZnO have a variety of unique properties which give it high potential on the photocatalysis, ZnO have some drawbacks which scale down its performance in photocatalysis. ZnO absorbs mainly the UV light which compromises a small portion

of the solar spectrum, and this makes it expensive when using external sources of UV light to excite the band gap of the ZnO in order to produce electron-hole pairs [10]. Also, the high recombination rate of $e-h$ in the ZnO prevent the path of electron-hole outward, and then reduce the photocatalysis efficiency. The greatest drawback is that ZnO NSs get photo-corrosion when immersed in solvent under the solar light due to hole trapping on the surface which is the most common issue for many NSs materials for photocatalysis. Many research works concerning overcoming these issues with ZnO to improve its photocatalysis performance through composite with other materials [10].

Furthermore, core-shell nanostructures have mainly been studied in terms of the enhancement of optical, electrical, thermal and catalytic properties with an emphasis on emergent behavior that occurs due to the nanoscale structure size and related quantum confinement effects. Examples include tunable photoluminescence in semiconductor/metal nanoparticles, improved dielectric properties of the composite nanoparticles, and size-dependent catalytic efficiencies in core-shell nanostructures. These enhanced properties are the result of a combination of the familiar size effects observed in nanomaterials due to the large surface to volume ratios role the core-shell structure plays in the applicable photonic, electronic, plasmonic, band-gap, and other interactions with in the core-shell nanostructures ($CSNSs$) [11]. Also, core-shell nanoparticles have unique structural features to achieve multi-functional properties. It received incredible research interests in recent years exhibiting improved and tailorable material properties [12].

The surface engineering of CSNSs is an important device to control the properties of the nanocrystals and in particular optical materials. One important technique is the overgrowth of nanocrystals with a shell of a second semiconductors, resulting in a CS systems [13]. Here, the method has been successfully applied to improve photo-oxidation stability by the proper choice of the core and shell material (i.e.,

ZnO as a core, Cu and Au as a shell), to tune the emission wavelength in a large spectral region. Nowadays, almost any type of core nanocrystals, prepared by a robust chemical synthesis methods has been over grown with shells of others noble metal materials. Depending on the band gaps and the relative position of electronics energy levels of the involved semiconductors, the shell have different functions in core-shell nanocrystals [13].

2.2 Quantum confinement effect and band gap

A nanostructure is simply any material with one or more spatial dimensions reduced to the nanometer scale. The Bohr radius of charge carriers in a semiconductor is on the order of a few tens of nanometers, (in ZnO, Cu, and Au). When one or more dimensions of a system are on par with this length scale, the carrier are said to be confined. A quantum dot is defined as a system confined in three dimensions. Therefore, a quantum dot has zero degrees of freedom, i.e., a quantum dot is $0D$ system. Similarly, a quantum wire (Q-wire) is confined in two dimensions ($1D$ system), and a quantum well (QW) is confined in one dimension ($2D$ system). Schematically, these definitions are illustrated in Fig. 2.1.

Moreover, quantum dots (QDs) have attracted great attentions since their unique optical properties related to quantum confinement products where their band gap can be tuned by adjusting their particle size. This effect gives a significant impact on the energy band gap of the QDs. As the size of the particles reaches nanoscale, the movement of excitons is impeded. However, the total energy of excitons is significantly unaffected until the size of particles is smaller than the exciton Bohr radius. At this point, the excitation energy required to create electron-hole pairs starts to increase, and this inversely proportional phenomenon of excitation energy [14].

Quantum confinement (QC) is defined as, a reduction in the freedom motion of the carrier particles, implying a reduction in the allowed phase space. This effect

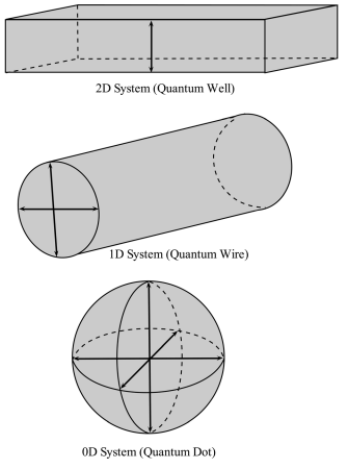

Figure 2.1: Schematic representation of quantum wells, wires, and dots. The arrows indicate the confinement axis. [14]

happens through the use of a confining potential due to band gap differences with a surrounding matrix material or with electric field gradients [15].

Quantum confinement generally results in a widening of the band-gap with a decrease in the size of the QDs. The band-gap in a material is the energy required to create an electron and a hole at rest (i.e., with zero kinetic energy) at a distance far enough apart that their Coulombic attraction is negligible. If one carrier approaches the other, they may form a bound electron-hole pair, i.e., an exciton, whose energy is a few meV lower than the band-gap [16]. The distance between the electron and hole is called the exciton Bohr radius (r_B). If m_e and m_h are the effective masses of electron and hole, respectively, the exciton Bohr radius for bulk semiconductor can be expressed by Eq. (2.2.1), where ϵ, $\hbar$, and e are the optical dielectric constant, reduced Planck's constant, and the charge of an electron, respectively. That is,

$$r_B = \frac{\epsilon \hbar^2}{e^2}\left(\frac{1}{m_e} + \frac{1}{m_h}\right). \tag{2.2.1}$$

If the radius (r) of a quantum dot approaches r_B, i.e., $r \approx r_B$ or $r < r_B$ the motion of the electrons and holes are confined spatially to dimension of the QDs which causes

an increase of the excitonic transition energy and the observed blue shift in the QD band-gap and luminescence.

2.2.1 Weak confinement regime

To describe this regime, the radius r of a crystallite should be greater than the bulk exciton Bohr radius r_B. In this region of confinement of week, the dominant energy is the Coulomb term and its already occurs a size quantization of the exciton motion. Binding energy of exciton states are shifted to higher energies by confinement and the shift in energy ΔE is proportional to $1/r^2$. The shift 'ΔE' of the exciton ground state is given approximately by [14]

$$\Delta E \approx \frac{\hbar^2 \pi^2}{2Mr^2}, \tag{2.2.2}$$

where M is the mass of the exciton and it is given by $M = m_e^* + m_h^*$, with m_e^* and m_h^* being the effective masses of the electron and hole, respectively.

2.2.2 Moderate confinement regime

The moderate confinement regime occurs when $r \approx r_B$ and $r_h < r_B < r_e$, where r_e is electron Bohr radii measures from electron to electron and r_h is the hole Bohr radii measures from hole to hole, respectively. In II-VI semiconductors, this region is well observable in small QDs. Its characteristic feature is the well restricted motion of a photo excited hole.

2.2.3 Strong confinement regime

Finally, the size of a QD can be decreased in such a way $r \ll r_B$ and $r \ll r_h$ and r_e in the strong confinement regime. The Coulomb term of electron-hole interaction is now small and can be ignored or treated as perturbation. The coloumbic interaction between electrons and holes can now be thought of as confinement independent particles. So excitons are does't formed and the separate size quantization of an electron

and hole is the dominant factor. The incident spectra consist also of a connects of lines due to the transition between sub-bands. This factor is confirmed experimentally and the simple model gives energy is shift as a function of crystallite size as

$$\Delta E \approx \frac{\hbar^2 \pi^2}{2\mu r^2}, \tag{2.2.3}$$

In which the exciton mass M is replaced by the reduced exciton mass μ, where

$$\mu = \frac{m_e^* m_h^*}{m_e^* + m_h^*}. \tag{2.2.4}$$

The electrons and holes in QDs are treated as independent atoms and from the excited state there exists a ladder of discrete energy levels, as in molecular systems.

2.3 Density of states

The density of states are different energy states that electrons are offered to occupy at a specific energy level, i.e., the number of electron state per unit energy per unit volume. The unit of density of state is expressed as $eV^{-1}cm^{-3}$ and it offers information on how the energy states are distributed in a given system. It is usually denoted as $g(E)$. Further, the density of states points to an enability of the number of states in a system which is important in determining the energy distribution of carrier and carrier concentration within a semiconductor [17]. The number of states achieved by a quantum system is the possible number of available states, which may mathematically be expressed as

$$N = \frac{V_{system}}{V_{single-states}} \times m, \tag{2.3.1}$$

where N represents the number of states, V_{system} represents the volume of the whole system, $V_{single-state}$ represents the volume of a single state of the system, and m is the number of atoms in the system.

In an excited state, the density of states depends on the energy gained by an electron. It is the first derivative of the state with respect to energy. It is mathematically expressed as

$$g(E) = \frac{\partial N}{\partial E} \tag{2.3.2}$$

For the bulk system ($3D$ systems) with momentum wave vector k: $N = k^2/3\pi$. For a $2D$ system (i.e., two degrees of freedom) $N = k^2/2\pi$. For a $1D$ system: $N = 2k/\pi$. For a $0D$ system, there is no k space to be filled and the number of density is discrete. These definitions lead to the following expression for the DOS:

$$g_{3D}(E) = \frac{1}{\pi^2}\left(\frac{m^*}{\hbar^2}\right)^{1/2}\sqrt{2E},$$

$$g_{2D}(E) = \frac{m^*}{2\hbar^2}\sum_{n_z}\Theta(E - E_{n_z}),$$

$$g_{1D}(E) = \frac{1}{\pi\hbar}\sqrt{2m^*}\sum_{n_z,n_y}\left(E - E_{n_z,n_y}\right)^{-1/2},$$

and

$$g_{0D}(E) = 2\sum_{n_x,n_y,n_z}\delta(E - E_{n_x,n_y,n_z}). \tag{2.3.3}$$

Here, m^* is the effective mass, $\Theta(E)$ is the step function, E is the energy of the particular state E_{n_i} with $i = x, y, z$ is the quantized energy of the particular confinement direction, and $E_{n_z,n_y} = E_{n_z} + E_{n_y}$, etc. To first order, in the infinite spherical potential confinement configuration, it is given by

$$E_{n_i} = \frac{\hbar^2\pi^2 n_i^2}{2m^* D_i^2}, \tag{2.3.4}$$

where n_i is the principle quantum number and D_i is the confinement diameter. Note that the energy in Eq. (2.3.4) is offset by the band gap energy E_g, in semiconductors.

Further, the density of states illustrates that a change in the confinement dimensions directly changes the energy occupation level. Thus, a modification in the density

of states with respect to the dimensions of the system is referred to as band gap engineering a device can be engineered to absorb or emit light at a tunable wavelength.

2.4 Plasmonic nanostructure

Plasmonic nanostructure is becoming an attractive field due to its potential applications in many areas. The plasmonic properties of noble metallic can be tuned by changing the size and shape of both the core and the overall particles. With efforts from scientists in different areas, plasmonic nanostructures are used in the optical device, photonic circuits and sensors as well as in medical diagnostics [18]. Furthermore, plasmonic nanostructures have met tremendous successes in nanoelectronics, chemistry, biology, physics, catalysis, electro-catalysis, and in biomedical field. Then, metallic coat core-shell structures had been successfully introduced to passivate the surface and tune the surface plasmon resonance wavelength [19].

2.4.1 Basic idea of the plasmonic resonance

An atoms consist of a positive core surrounded by an electron cloud. Due to the interaction of the atoms with the incident radiation, the electrons in the conduction band are shifted consequent of the force exerted by the external electric field. As the opposite charges are separated, the electric dipoles are induced as shown in Fig. 2.2.

The columbic interaction between the electrons and the protons acts as a restoring force which leads to electronic oscillations. These electronic collective oscillations of a metals are called plasmons [20]. When one metal particle is in a uniform electric field, the electron inside particle moves from one side to the other side. Then, the electrons will move back to the original position driven by the attractive force. As a result, the electrons will oscillate back and forth at a specific frequency, which is called plasma frequency. And plasmon is a quantization of these oscillation movements. Plasmon

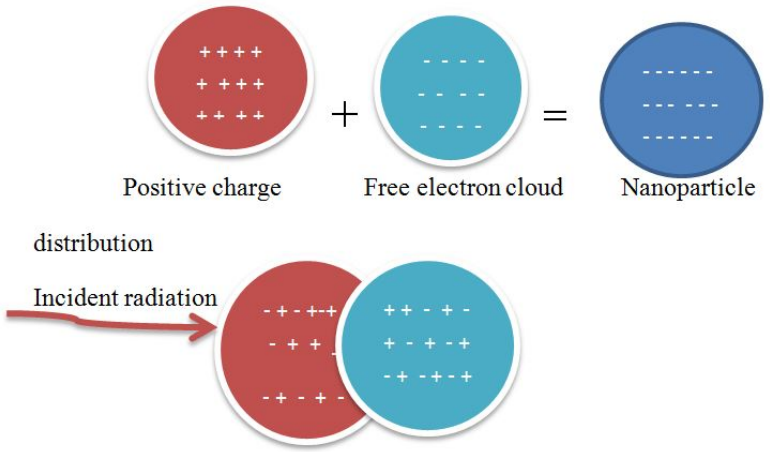

Figure 2.2: Schematic representation of the plasmon resonance.

materials have been playing an attractive role in the optical properties of metal nanostructures. Usually metals are highly reflective materials due to their plasma frequency which lies in the ultraviolet spectrum which is higher than the frequency of visible light. Metals such as silver, aluminum, copper and gold, had electronic inter-band transitions in the visible range, so they have their particular colors. The position and intensity of plasmon absorbance are highly affected by the surface property of the materials. For the surface features including modification of plasmonic structure's shape, morphology and size, they could build different plasmonic modes [20].

2.4.2 Types of electron resonance

The electronic fluctuations are classified into SPR and LSPR according to the spatial distribution of the negative charges. In the former case, the alternating negative/positive charges along the system surface generate a propagating electronic density wave in a direction parallel to the dielectric/metal interface. The propagating length depends on the dielectric function of the metal and the wavelength of the exciting radiation. The free-space light initial is unable to excite the SPR, because of the mismatch in the momentum between the incident light and the SPR. The

excitation of the SPR requires an additional momentum which can be achieved by using the idea of the total internal reflection in the metallic surface [21]. Also, surface plasmons are a coherent vibration charge carriers in conduction on a metal surface excited by an electromagnetic wave on the metal nanostructures. These free conduction electrons have their own oscillation frequency, which is called surface plasmon resonance frequency (SPRF) [22]. SPR was dependent on the size and shape of the nanostructures. When the light irradiate on such metal nanostructures (the light is an electromagnetic wave with its own oscillating frequency), the negative carrier will resonate with the light when SPR frequency and light frequency match. Therefore, the incident light at SPR frequency will strongly be absorbed and scattered. In other words, the electric field of incident light will be enhanced [22].

For metal nanoparticles, if the wavelength of the light greater than the size of nanoparticles, the collective oscillation of plasma would be localized near the surface. Also the resonance frequency would shift from the plasma frequency to the surface plasmon resonance frequency. For metals including Au, Ag, and Cu surface plasmon resonance (SPR) peaks of their nanoparticles are in the visible region. At SPR frequency, these nanoparticles strongly enhance the scattering and absorption of the visible lights [20].

If the electronic fluctuations occur locally around the nanoparticle, the corresponding surface oscillation is called local surface plasmon resonance (LSPR). The confined electronic vibrations in the LSPR enhance the local field distribution at the surface of the nanostructures [21].

The best way to explain localized surface plasmon resonance (LSPR) is probably by considering the case of a metallic sphere embedded in a host medium. The conduction electrons of this sphere are displaced analog to the free electron gas models.

Because the conduction electrons are confined to the sphere (localized), an effective restoring force counteracts any displacement. In contrast to the surface plasmon resonance, localized surface plasmon resonance is a non-propagating excitation. This fact automatically gives the main difference between localized surface plasmon resonance and surface plasmon resonance; because localized surface plasmons are non-propagating excitations, there is no wave vector matching problem and localized surface plasmon resonance can be excited by direct light illumination [22].

Local surface plasmon resonances also can be excited in bound geometry such as metallic nanoparticles. Such a plasmon is called a localized surface plasmon. Its frequency can be determined using the electrostatic approximation by solving the boundary conditions of Maxwell's equations. Since a nanoparticle's size is very small compared to the wavelength of light. Localized surface plasmons can be resonance excited with light of the appropriate frequency irrespective of excitation light wave vector. Therefore, localized surface plasmons also effectively decay with light radiation. Since localized surface plasmons are confined to the particle, this results in a significant incident of light field enhancement at small metallic particles due to the small volume of the localized surface plasmon mode [20, 22].

2.4.3 Tunability of plasmon resonance

As we know optical properties of the metallic nanoparticles depend strongly on the structural parameters (size and shape), type of the metal and the dielectric function of the surrounding material where they are embedded. Other parameters that have a dramatic effect on their optical response are the coupling between the plasmonic resonances in near by structures, the orientation of the particles compare to the incident radiation, and the polarization state of the incident light. By tuning these variables, the optical properties of LSPR modes can be varied over the entire UV-Visible spectral regions [23].

2.4.4 Size effect on the plasmon oscillations

The surface plasmon resonance is mainly affected by particle size, shape as well as the surrounding environment. The size effect influencing the surface plasmon resonance are divided into extrinsic and intrinsic. The extrinsic size effect is a retardation effect due to the excitation of multipolar plasmon modes when nanoparticle size is increased toward the resonant electromagnetic wavelength. The extrinsic size effect is a bare electromagnetic phenomenon appearing in the optical absorption spectrum as broadening and shift of the surface plasmon resonance for increasing metal nanoparticle size. Intrinsic size effects are due to the modification of the metal optical constant when metallic nanoparticle size is below 50 nm. The optical constant varies since additional contributions to the free electron relaxation when the nanoparticle size is reduced. In particular, the free electron scattering at particle size surface is no more negligible when conduction electrons mean free path ($\sim 40\ nm$) for copper (Cu) and gold (Au) nanoparticles becomes comparable the particle size [21].

The use of the metallic nanostructure in the technical applications requires shape and size controlled composite methods. A frequency of resonance is a strong function of the particle size such that the latter controls the spatial distribution of the polarization charges over the surface and the negative/positive charges separation as well. In the quasi-static approximation, the observed LSPR modes are attributed to the excitation of the dipolar resonance modes. As the size increases, the resonance wavelength the observed plasmon band increases due to reduce in the restoring force between the opposite charges [22].

2.5 Models of dielectric function

The dielectric function $\epsilon(\omega, k)$ of the electrons is strong dependent on frequency and wave vector. When an electromagnetic wave interacts with matter it exerts a force

by electric fields $\vec{E}$ on the electrons in the matter. At high frequencies the electric field $\vec{E}$ can displace the electrons in the atom. As a result each atoms becomes an electric dipole with dipole moment $\vec{p}$ and the total number of dipole moment per unit volume is known as polarization. The dielectric function is directly related to the electric field $\vec{E}$, the polarization $\vec{P}$, and the dipole moment density $\vec{p}$ [24]. The physical understanding of light spans by small particles begins with the electric dipole concept. The total dipole moment per unit volume is polarization of materials exposed to electromagnetic fields is determined by dielectric function. The function of dielectric for metal particles are decomposed into two parts. The first component is the Drude free electron term and the else part is the substantial contribution of the inter-band charges by Lorentz-Drude model and is expressed as [25]:

$$\vec{P} = \chi_e \epsilon(\omega) \vec{E}(\omega). \tag{2.5.1}$$

Further, important example for a response function is the relationship between the displacement $\vec{D}$ and an applied field $\vec{E}$. That is,

$$\vec{D(\omega)} = \epsilon(\omega) \vec{E}(\omega), \tag{2.5.2}$$

where $\epsilon(\omega)$ is known as the dielectric function or relative permittivity of the system.

2.5.1 Drude's dielectric model

The first approximation to metal dielectric function is based on the so called Drude model, which considers that electrons in a metal are basically free and can be forced to oscillation when an electromagnetic wave of frequency ω is incident upon it [21]. This model deals about electrons not bounded to a particular nucleus. Because these conduction electrons are not bound there is no elastic restoring forces so k_{spring} and $\omega_0 = 0$. In the general case of the real bulk metals, the dielectric function consists of two contributions accounting for the inter-band and intra-band electron transitions.

That involves the bound and the free electrons, respectively. The contribution of the intra-band transition can be described by using the Drude free electron model. The equation of the motion of free electrons of an effective mass (m) and charge (e) in a sinusoidal electric field ($E(t)$) of angular frequency (ω), can be expressed as

$$m\left(\frac{\partial^2\vec{r}}{\partial t^2}+\Gamma\frac{\partial\vec{r}}{\partial t}\right)=-e\vec{E}. \tag{2.5.3}$$

Assume that $\vec{r}$ and $\vec{E}$ are harmonically time dependent and has the form $\vec{r}=\vec{r_0}e^{-i\omega t}$ and $\vec{E}=\vec{E_0}e^{-i\omega t}$, respectively; then equation (2.5.3) can be written as:

$$\Big(-\omega^2-i\Gamma\omega\Big)\vec{r}=-\frac{e\vec{E}}{m}, \tag{2.5.4}$$

or,

$$\vec{r}=\frac{e\vec{E}}{m\Big(\omega^2+i\Gamma\omega\Big)}. \tag{2.5.5}$$

The dipole moment of one electron is given by

$$\vec{p}=-e\vec{r}=\frac{-e^2\vec{E}}{m\Big(\omega^2+i\Gamma\omega\Big)}. \tag{2.5.6}$$

Dipole moment per unit volume is polarization. That is;

$$\vec{P}=n\vec{p}=\frac{-ne^2\vec{E}}{m\Big(\omega^2+i\Gamma\omega\Big)}, \tag{2.5.7}$$

where n is the electron concentrations. The dielectric function $\epsilon(\omega)$ at frequency ω is

$$\epsilon(\omega)=\frac{\vec{D}(\omega)}{\vec{E}(\omega)}=1+4\pi\frac{P(\omega)}{\vec{E}(\omega)}. \tag{2.5.8}$$

The dielectric function of free electrons follows from equation (2.5.7) and (2.5.8). That is,

$$\epsilon(\omega)=\epsilon_\infty-\frac{\omega_p^2}{\omega^2+i\Gamma\omega}. \tag{2.5.9}$$

Equation (2.5.9) is well known as the Drude dielectrics model. The real $\epsilon_1(\omega)$ and imaginary $\epsilon_2(\omega)$ part of the complex permittivity $\epsilon(\omega)$ in equation (2.5.9) are given by

$$\epsilon_1(\omega) = \epsilon_\infty - \frac{\omega_p^2}{\omega^2 + \Gamma^2},$$

and

$$\epsilon_2(\omega) = \frac{\omega_p^2 \Gamma}{\omega\left(\omega^2 + \Gamma^2\right)}.$$

The condition above are verified if Γ parameters are negligible. ω_p and Γ are the most important parameters in the Drude model. Both ω_p and Γ are influencing the real and imaginary parts of the complex permittivity. The equation

$$\omega_p = \left(\frac{4\pi n e^2}{m}\right)^{\frac{1}{2}} \tag{2.5.10}$$

is the electron plasma frequency. The plasma frequency ω_p of the metal is strongly temperature dependent and as ω_p increases the amplitude of $\epsilon_1(\omega)$ and $\epsilon_2(\omega)$ increase too.

2.5.2 Lorentz-harmonic oscillator model

The Lorentz oscillator model, also known as the Drude-Lorentz oscillator model, involve modeling an electron as a driven damped oscillator. In this model the electron is connected to the nucleus transition a hypothetical spring with spring constant k_{spring}. The driving force is the oscillator electric field. The source of the damping force is not specified, but is present so that the oscillator don't go infinite when the driving force is at the resonate frequency. A target of this model is to (a) use Newton's 2^{nd} law to obtain the motion of the electron, which (b) can then be used to obtain expression for the dipole moment, polarization, and dielectric constant [26].

From the force balance, the equation of motion for an electron bounded by a

harmonic force and acting on by an electric field is

$$F_{inertia} + F_{damping} + F_{replusive} = F_{electrical}, \tag{2.5.11}$$

or quantitatively becomes

$$m\left(\frac{\partial^2 \vec{r}}{\partial t^2} + \Gamma \frac{\partial \vec{r}}{\partial t} + \omega_0^2 \vec{r}\right) = -e\vec{E}, \tag{2.5.12}$$

where Γ is the damping constant, $\omega_0 = \sqrt{k_{spring}/m}$ is the resonance frequency of the bound electron natural frequency, and k_{spring} is the spring constant. Suppose that the applied electric field varies harmonically with time according to the factor, $e^{i\omega t}$, that is $\vec{E} = \vec{E}_0 e^{i\omega t}$. And assuming that the motion of the electron has the same time dependence that is $\vec{r} = \vec{r}_0 e^{i\omega t}$ we can find that

$$\left(\omega_0^2 - \omega^2 + i\Gamma\omega\right)\vec{r} = \frac{-e\vec{E}}{m}, \tag{2.5.13}$$

or,

$$\vec{r} = \frac{-e\vec{E}}{m\left(\omega_0^2 - \omega^2 + i\Gamma\omega\right)}. \tag{2.5.14}$$

The dipole moment contribution for one electron is given by

$$\vec{p} = -e\vec{r} = \frac{e^2\vec{E}}{m\left(\omega_0^2 - \omega^2 + i\Gamma\omega\right)}, \tag{2.5.15}$$

and the corresponding polarization $\vec{P}$ is

$$\vec{P} = n\vec{p} = \frac{ne^2\vec{E}}{m\left(\omega_0^2 - \omega^2 + i\Gamma\omega\right)}. \tag{2.5.16}$$

If there are n molecules per unit volume with f_i electrons per unit molecules with binding frequency ω_i and damping constant Γ_i, the polarization given by Eq. (2.5.16) becomes

$$\vec{P} = \frac{ne^2\vec{E}}{m}\sum \frac{f_i}{\omega_i^2 - \omega^2 + i\omega\Gamma}. \tag{2.5.17}$$

The dielectric function $\epsilon(\omega)$ is

$$\epsilon(\omega) = \frac{\vec{D}(\omega)}{\vec{E}(\omega)} = 1 + \frac{4\pi\vec{P}(\omega)}{\vec{E}(\omega)}. \tag{2.5.18}$$

The dielectric function of the electron follows from equation (2.5.17) and (2.5.18).

$$\epsilon(\omega) = 1 + \sum \frac{f_i\omega_p^2}{\omega_i^2 - \omega^2 + i\omega\Gamma}, \tag{2.5.19}$$

where $\omega_p^2 = 4\pi ne^2/m$ is the plasma frequency. Equation (2.5.19) is known as Lorentz harmonic oscillator model.

Chapter 3

The Model - Spherical Core-Shell Nanostructures

3.1 Theoretical model and calculation

Modeling of spherical core-shell nanostructure is shown in Fig. 3.1. In this spherical core-shell nanostructure, there are two interfaces: core@shell and shell@host matrix. In this study, the system will be modeled as a meta-material consisting of a semiconductor core, metallic shell embedded in a dielectric host matrix. Here, the host matrix found outside the core-shell nanostructure, therefore will be modeled as an infinite medium where potential is induced [27]. The optical as well as the plasmonic properties of two layer nanoparticles can be successfully describe within the framework of classical electrodynamics of a continuous medium [28]. Consider an array of a spherical core-shell composite nanoparticles consisting of a semiconductor core dielectric function ϵ_c, and a metallic shell dielectric function ϵ_s embedded in a dielectric function of host matrix. Assume that the host medium is an isotropic and non-absorbing with dielectric function ϵ_h [29].

As shown in Fig. 3.1, region 1 is the core characterized by radius r_c and dielectric function. Also, the shell material has a thickness $t_{s,Cu,Au}$ (i.e., $t_{s,Cu,Au} = r_{s,Cu,Au} - r_c$), with a total radius $r_{s,Cu,Au}$, and the dielectric function. It is important to note that

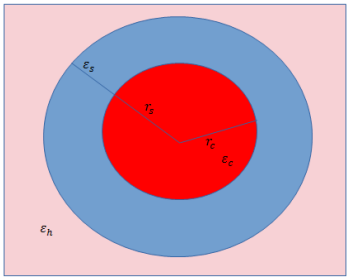

Figure 3.1: Model of $ZnO@Cu$ and $ZnO@Au$ spherical core-shell nanostructures.

none of the dielectric functions ϵ_i $(i = c, s, h)$ have been specified. Each can have real and imaginary components, while the dielectric function of the core (ϵ_c) and the embedding medium dielectric function (ϵ_h) are assumed to be real constant, therefore the geometry becomes that of a metal nanoshell when ϵ_s is specified as the dielectric function of a metal and the core is nominally a dielectric material [30, 31].

The general solution of the Laplace equation, the electric potential for each region is given by the following equations:

$$\Phi_i(r, \theta) = \left(C_i r + \frac{B_i}{r^2}\right) cos\theta, \tag{3.1.1}$$

where the coefficient C_i and B_i are to be determined from the boundary conditions.

In particular, consider the composite of two layer spherical core-shell nanocomposite that is irradiated with an incident light. As a result of this light, electric field is induced in the system due to polarization. The distribution of the electrostatic potential Φ associated with the induced electric field inside and outside of the system can be obtained by solving the Laplace equations $\nabla^2\Phi = 0$, in spherical coordinates. In addition, the wavelength of the incident electromagnetic radiation is much greater than a typical size of the system. Therefore, the distribution of the potential in a spherical metal nanoparticles with a dielectric core embedded in a dielectric host matrix in an external constant electric field can be described by the following expressions

[31, 32, 33].

$$\Phi_c(r,\theta) = C_1 r\cos\theta \qquad r \le r_c \tag{3.1.2}$$

$$\Phi_s(r,\theta) = \left(C_2 r + \frac{B_2}{r^2}\right)\cos\theta \qquad r_c \le r \le r_s \tag{3.1.3}$$

$$\Phi_h(r,\theta) = \left(C_3 r + \frac{B_3}{r^2}\right)\cos\theta \qquad r \ge r_s, \tag{3.1.4}$$

where Φ_c, Φ_s and Φ_h are the electric potentials obtained for the core, shell, and host matrix, respectively; the quantity C_3 is associated with the external applied field, r and θ are the coordinates of the sphere and at the interface of the composite the coefficients C_1, C_2, B_2, and B_3 can be determined by using the appropriate boundary conditions.

With C_3 and B_1 determined, applications to equation (3.1.1), results in a set of four equations and four unknowns that can be solved, then the electric field in each region can be obtained with $E_i = -\nabla\Phi_i(r,\theta)$ [30].

Note that the second term on the right side of equation (3.1.4), represents the induced potential outside the core-shell nanoparticles. The optical properties of these system may be described by the induced field outside the concentric sphere, as a result it is suffice to determine the values of the coefficient B_3; magnificent the relevant boundary condition in equation (3.1.2)-(3.1.4), we obtains the following relations [31].

$$B_3 = \left[\frac{\big(\epsilon_c + 2\epsilon_s\big)\big(\epsilon_s - \epsilon_h\big) + \rho\big(\epsilon_c - \epsilon_s\big)\big(2\epsilon_s + \epsilon_h\big)}{\big(\epsilon_c + 2\epsilon_s\big)\big(\epsilon_s + 2\epsilon_h\big) + 2\rho\big(\epsilon_c - \epsilon_s\big)\big(\epsilon_s - \epsilon_h\big)}\right] C_3 r_s^3, \tag{3.1.5}$$

$$B_3 = \frac{\big(\epsilon_s - \epsilon_h\big) + \rho\big(2\epsilon_s + \epsilon_h\big)x}{\big(\epsilon_s + 2\epsilon_h\big) + 2\rho\big(\epsilon_s - \epsilon_h\big)x} r_s^3 C_3, \tag{3.1.6}$$

where

$$\rho = \left(\frac{r_c}{r_s}\right)^3,$$

and

$$x = \frac{\epsilon_c - \epsilon_s}{\epsilon_c + 2\epsilon_s}.$$

Hence, from Eq. (3.1.4) we find that the induced potential outside the concentric spheres is given by

$$\Phi_{ind} = \frac{B_3}{r^2}\cos\theta. \tag{3.1.7}$$

Moreover, employing the dipole approximation the induced potential may also be expressed as [34]

$$\Phi_{ind} = \frac{\vec{p}\cos\theta}{4\pi\epsilon_h r^2}, \tag{3.1.8}$$

where $\vec{p}$ is the magnitude of the system's electric dipole moment. In view of equation (3.1.7) and (3.1.8), the dipole moment becomes

$$\vec{p} = 4\pi\epsilon_h B_3 = \epsilon_h \alpha C_3. \tag{3.1.9}$$

For a concentric spherical core-shell particles embedded in a host matrix of permittivity ϵ_h, we calculate the polarizability by solving Laplace's equation in the spherical coordinate with the boundary conditions that the potential and the normal displacement vectors must be continuous at the boundary between the particle and the host medium applying to core-shell system leads to the following expression for polarization [35]:

$$\alpha = 4\pi r_s^3\left[\frac{\big(\epsilon_c + 2\epsilon_s\big)\big(\epsilon_s - \epsilon_h\big) + \rho\big(\epsilon_c - \epsilon_s\big)\big(2\epsilon_s + \epsilon_h\big)}{\big(\epsilon_c + 2\epsilon_s\big)\big(\epsilon_s + 2\epsilon_h\big) + 2\rho\big(\epsilon_c - \epsilon_s\big)\big(\epsilon_s - \epsilon_h\big)}\right]. \tag{3.1.10}$$

We would like to note that the polarizability of two layer spherical inclusions may be represented in the following form:

$$\alpha = 4\pi r_s^3 \frac{\epsilon_I - \epsilon_h}{\epsilon_I + 2\epsilon_h}. \tag{3.1.11}$$

Using equations (3.1.10) and (3.1.11), we get the inclusion dielectric function (DF) of the core-shell spherical to be

$$\epsilon_I = \epsilon_s \frac{\Big(\epsilon_c + 2\epsilon_s\Big) + 2\Big(\epsilon_c - \epsilon_s\Big)\rho}{\Big(\epsilon_c + 2\epsilon_s\Big) - \Big(\epsilon_c - \epsilon_s\Big)\rho}, \tag{3.1.12}$$

where β is the volume fraction of a spherical core-shell nanostructures in the inclusion particle defined by

$$\beta = 1 - \rho = 1 - \left(\frac{r_c}{r_s}\right)^3. \tag{3.1.13}$$

Using equations (3.1.12) and (3.1.13), we can write the inclusion dielectric function of a system as

$$\epsilon_I = \epsilon_s \frac{\epsilon_c\left(\frac{3}{\beta} - 2\right) + 2\epsilon_s}{\epsilon_c + \epsilon_s\left(\frac{3}{\beta} - 1\right)}. \tag{3.1.14}$$

Effective medium theory and Clausius-Mossoti equation for a composite with spherical core-shell have the form [36]

$$\frac{\epsilon_{eff} - \epsilon_h}{\epsilon_{eff} + 2\epsilon_h} = \frac{n\alpha}{3}, \tag{3.1.15}$$

where ϵ_{eff} is the effective permittivity, n is the number in the inclusion system and α is the polarizability defined by equation (3.1.11). Further equation (3.1.11), may conveniently be rewritten as

$$\alpha = 4\pi r_s^3 \eta,$$

where η is the dimensionless polarizability defined by

$$\eta = \frac{\epsilon_I - \epsilon_h}{\epsilon_I + 2\epsilon_h}. \tag{3.1.16}$$

Equation (3.1.14) is substituted into equation (3.1.16), and rearranged, we get

$$\eta = \frac{\epsilon_c\epsilon_s\left(\frac{3}{\beta} - 2\right) + 2\epsilon_s^2 - \epsilon_c\epsilon_h - \epsilon_s\epsilon_h\left(\frac{3}{\beta} - 1\right)}{\epsilon_c\epsilon_s\left(\frac{3}{\beta} - 2\right) + 2\epsilon_s^2 + 2\epsilon_c\epsilon_h + 2\epsilon_s\epsilon_h\left(\frac{3}{\beta} - 1\right)}. \tag{3.1.17}$$

Maxwell-Garnett mixing formula for the spherical core-shell of our study interest is given by

$$\epsilon_{eff} = \epsilon_h\left[\frac{1 + 2\eta\xi}{1 - \eta\xi}\right], \tag{3.1.18}$$

where ξ is the filling factor of the spherical core-shell inclusion given by

$$\xi = \frac{4\pi n r_s^3}{3}. \tag{3.1.19}$$

It is worthwhile to note that equations (3.1.17) and (3.1.18) are general expressions for any two-layered spherical core-shell composite nanoparticle that are embedded in a dielectrics host matrix, regardless of either the core-shell composites are metals, semiconductors-dielectrics or a combination.

Chapter 4

Results and Discussion

It is well known that the optical properties of metal coated nanostructured metamaterials depends on their size, shape, the type of the metal coat, as well as the surrounding environment, i.e., the host medium. In our case, we will investigate theoretically and numerically the dependence of the optical properties of systems that consist of spherical $ZnO@Cu$ and $ZnO@Au$ core-shell quantum dots embedded in vacuum using an important parameters like quantum dots QDs size of core, the thickness of the shell, and the filling factor.

4.1 Dielectric function of the metallic shell

Below, we consider systems that consist of spherical $ZnO@Cu$ and $ZnO@Au$ core-shell quantum dots embedded in vacuum ($\epsilon_h = 1$). In the frequency domain of interest, the dielectric function (DF) of the ZnO core (ϵ_c) and the embedding medium (ϵ_h) are assumed to be real constants, while the dielectric function of the metallic sheet ($\epsilon_{s,Cu,Au}$) is chosen to have the modified Durde form that takes into account of the size of the quantum dots (QDs). That is,

$$\epsilon_{s,Cu,Au} = \epsilon_\infty - \frac{\omega_p^2}{\left[\omega^2 + i\omega\Gamma(r)\right]}, \tag{4.1.1}$$

where ϵ_∞ is the high-frequency permittivity which depends on the types of metal coat, ω_p is the electron plasma frequency of the metal shells, $\Gamma(r)$ is the size-dependent electron collision frequency, and ω is the frequency of the incident radiation. Also, the size-dependent damping parameter for copper and gold shells can be expressed as:

$$\Gamma_{Cu,Au}(r) = \Gamma_{0,Cu,Au} + A\frac{v_{f,Cu,Au}}{r}, \tag{4.1.2}$$

where $\Gamma_{0,Cu,Au}$ is the bulk frequency for copper or gold, which are related to dissociative losses. In addition, the velocities of electrons in copper and gold metals are denoted by $v_{f,Cu,Au}$, above the Fermi level, r is the electron mean free path, and A is a dimensionless constant that accounts for the depth of the electron scattering process at the interface [37].

From Eq. (4.1.1), the real $\epsilon_{s1,Cu,Au}$ and imaginary $\epsilon_{s2,Cu,Au}$ parts of the dielectric function can be separated as follows:

$$\epsilon_{s,Cu,Au} = \epsilon_{s1,Cu,Au} + i\epsilon_{s2,Cu,Au}, \tag{4.1.3}$$

where

$$\epsilon_{s1,Cu,Au} = \epsilon_\infty - \frac{\omega_p^2}{\omega^2+\Gamma^2} \quad \text{and} \quad \epsilon_{s2,Cu,Au} = \frac{\Gamma\omega_p^2}{\omega\left(\omega^2+\Gamma^2\right)}. \tag{4.1.4}$$

4.2 Numerical analysis

Consider the numerical evaluations of systems that consist of spherical $ZnO@Cu$ and $ZnO@Au$ core-shell quantum dots (QDs) embedded in vacuum with $\epsilon_c = 8.5$ and $\epsilon_h = 1$). Moreover, the other parameters used for the numerical evaluations are the following: $\Gamma_0 = 0.092\ eV$ and $\Gamma_0 = 0.072\ eV$ for the bulk damping constants of copper and gold, respectively; the velocities of electrons in copper and gold metals

are $v_f = 1.57 \times 10^6\ m/s$ and $v_f = 1.40 \times 10^6\ m/s$, respectively; the size dependent parameters are $\Gamma = 1.4 \times 10^{14}\ rad/s$ and $\Gamma = 1.1 \times 10^{14}\ rad/s$, respectively; the value of dimensionless constant is $A = 1$; the electron plasma frequencies for copper and gold, respectively, are $\omega_p = 1.34 \times 10^{16}\ rad/s$, and $\omega_p = 1.38 \times 10^{16}\ rad/s$. Also, $\epsilon_\infty = 12.076$ and $\epsilon_\infty = 11.575$ for copper and gold, respectively.

4.2.1 Refractive index

The refractive index n is the ratio of the speed of light (c) in vacuum to the speed of light (v) in a given medium, i.e., ($n = c/v$). The response of a medium to an incident electromagnetic wave may be described by a complex refractive index ($\tilde{n}$), which for a non-magnetic medium is defined [38].

$$\tilde{n} = \sqrt{\epsilon_{eff}}, \tag{4.2.1}$$

Given the fact that $\epsilon_{eff} = \epsilon_1 + i\epsilon_2$ is the complex effective dielectric function of the medium [39]. Introducing the real (n_1) and imaginary parts (n_2), $\tilde{n}$ may be written as;

$$\tilde{n} = n_1 + in_2 \tag{4.2.2}$$

Then, by equating their real and imaginary parts, we obtains the following equations of systems:

$$\epsilon_1 = n_1^2 - n_2^2 \quad \text{and} \quad \epsilon_2 = 2n_1n_2. \tag{4.2.3}$$

The solution of a system in Eq. (4.2.3), written in terms of n_1 and n_2 takes the following form:

$$n_1 = \frac{1}{\sqrt{2}}\left[\left(\epsilon_2^2 + \epsilon_1^2\right)^{\frac{1}{2}} + \epsilon_1\right]^{\frac{1}{2}}, \tag{4.2.4}$$

and

$$n_2 = \frac{1}{\sqrt{2}}\left[\left(\epsilon_2^2 + \epsilon_1^2\right)^{\frac{1}{2}} - \epsilon_1\right]^{\frac{1}{2}}. \tag{4.2.5}$$

Below, we present numerical plots of the real and imaginary parts of the refractive index of systems consisting of spherical $ZnO@Cu$ and $ZnO@Au$ core-shell nanostructures embedded in vacuum. The graphs are plotted by using Eqs. (4.2.4) and (4.2.5) with ϵ_{eff} given by Eq. (3.1.18).

A. Refractive index as a function of volume fraction, β

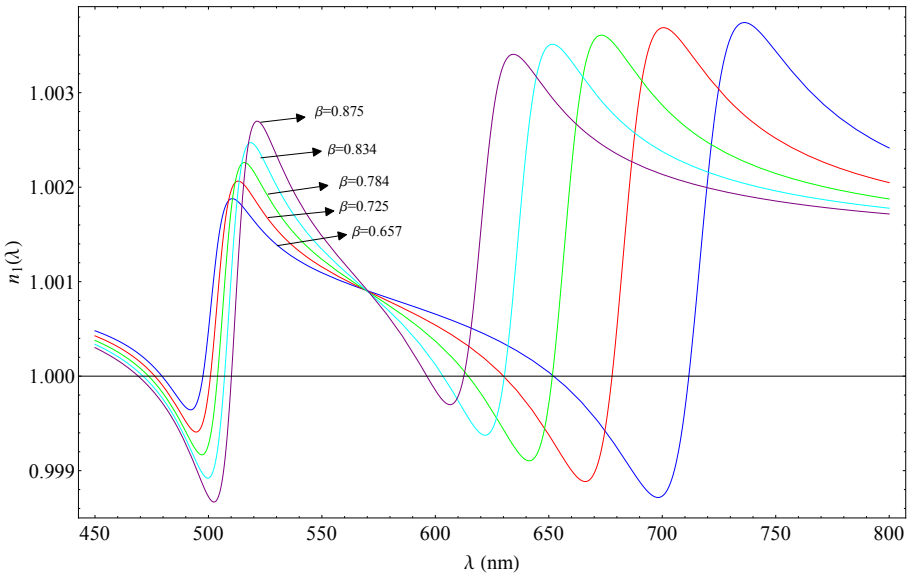

Figure 4.1: The real part of the refractive index of system of spherical $ZnO@Cu$ core-shell QDs embedded in vacuum as a function of wavelength for different values of β and a fixed value of ξ.

Figures. 4.1 and 4.2 depict the graphs of the real parts of the refractive index of systems of spherical $ZnO@Cu$ and $ZnO@Au$ core-shell quantum dots embedded in vacuum plotted as a function of the wavelength of the incident radiation for different values of volume fraction, β. It is observed that there are two sets of resonance peaks, both in the visible spectral region: the first set of peaks is located in the vicinity of (i) 515 nm and 490 nm for systems of $ZnO@Cu$ and $ZnO@Au$ quantum dots (QDs), respectively, while the second set of peaks are those located above the wavelength of (ii) 635 nm and 605 nm for systems of $ZnO@Cu$ and $ZnO@Au$ core-shell quantum

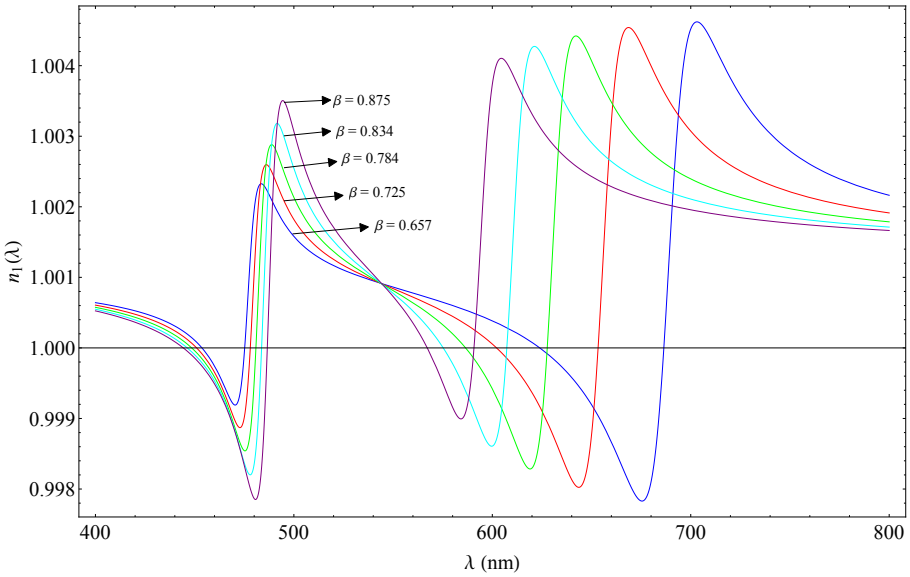

Figure 4.2: The real part of the refractive index of system of spherical $ZnO@Au$ core-shell QDs embedded in vacuum as a function of wavelength for different values of β and a fixed value of ξ.

dots (QDs), respectively. In both cases, the first set of peaks arises due to resonances at the inner (core/metal) interface and the second set of peaks are due to resonances at the outer (metal/medium) interface. When the values of the volume fraction β is increased, the first set of peaks shows slight red shift, while the second set of peaks are blue shifted (i.e., shifted towards higher energy values). In addition, when β is changed both sets of resonance peaks gets split. In particular, when the values of β is increased, the two resonance peaks gets closer and closer to one other and eventually merge for $\beta = 1$. For both $ZnO@Cu$ and $ZnO@Au$ systems of quantum dots (QDs), the first set of peaks are smaller in magnitude than the corresponding second set of peaks for a given value of β.

Comparisons Figs. 4.1 and 4.2 presents the spectra of refractive index of real parts calculated from Eq. (4.2.4) using the dielectric functions of bulk copper (Cu) and gold (Au) with $\epsilon_h = 1$ (vacuum) and $r_s = 30\ nm$. The gold nanoparticles presents a sharp plasmon resonance peak at $\lambda = 510\ nm$ with a maximum values $n_1 = 1.004$

at the plasmon resonance. In the case of the copper (Cu) nanoparticles, such a sharp peak is not observed, instead there is a broad band with a maximum values $n_1 = 1.003$ at $\lambda = 540\ nm$. The absence of sharp resonance is due to the damping of the plasmon excitation by inter band transitions for copper. Again as can be seen the graph there is always a certain a core to shell ratio that determines the maximum value of the surface plasmon resonance in any desired wavelength. The position of the plasmon resonance peak of Au and Cu nanoshell can be selectively tuned from $400 - 740\ nm$ and $450 - 760\ nm$, respectively. In brief, comparison of Figs. 4.1 and 4.2 show that (i) for a given value of β the resonance peaks for $ZnO@Cu$ quantum dots (QDs) occur at a higher wavelength than that of the $ZnO@Au$ quantum dots (QDs) system; which is attributed to the high value of ϵ_∞ for Cu than that of Au; and (ii) both sets of resonance peaks are more pronounced for $ZnO@Au$ quantum dots (QDs) system than that of $ZnO@Cu$ quantum dots (QDs) system, which is due to the relatively low value of the damping constant of Au.

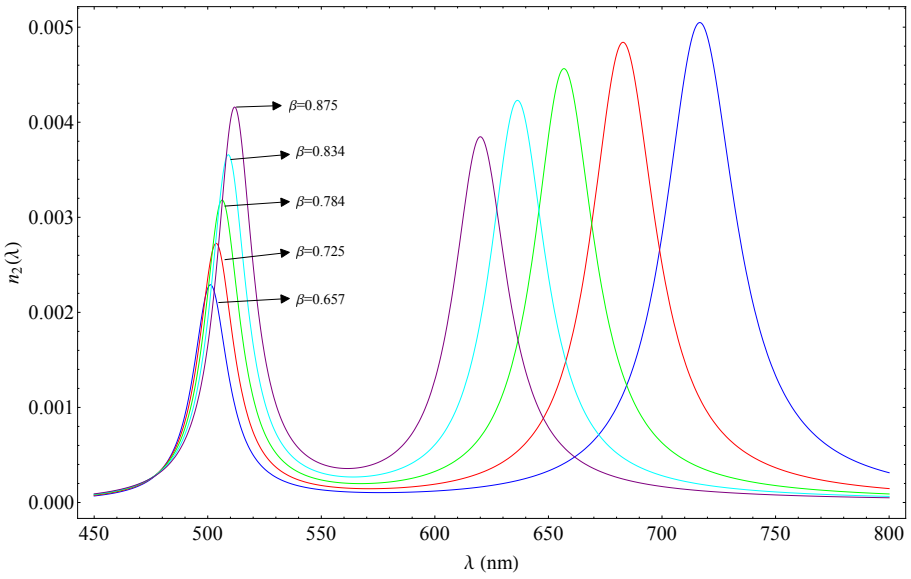

Figure 4.3: The imaginary part of the refractive index of system of spherical $ZnO@Cu$ core-shell QDs embedded in vacuum as a function of wavelength for different values of β and a fixed value of ξ..

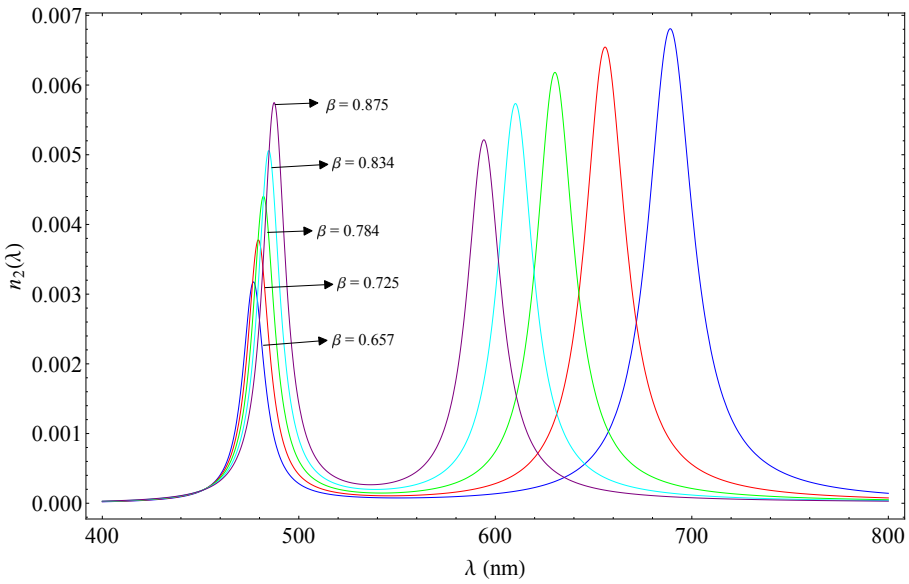

Figure 4.4: The imaginary part of the refractive index of system of spherical $ZnO@Au$ core-shell QDs embedded in vacuum as a function of wavelength for different values of β and a fixed value of ξ.

The graphs of the imaginary parts of the refractive index of systems of spherical $ZnO@Cu$ and $ZnO@Au$ core-shell quantum dots embedded in vacuum plotted as a function of the wavelength of the incident radiation for different values of volume fraction, β, are shown in Figs. 4.3 and 4.4. It is seen that the imaginary part of the refractive index possesses two resonances peaks for each system of quantum dots (QDs): the first set of peaks are found around 505 nm and 480 nm, and the second set of peaks are found above 620 nm and 595 nm to both copper and gold metals, respectively. The second set of peaks shows blue shifts when the volume fractions of the concentric spheres are increased, while the first set of resonance peaks show slight red shifts when the values of volume fraction is increased. In addition, when the values of β is decreased, the values of the first maxima are smaller than that of the corresponding second maxima. As it is observed from the graphs, the positions and values of the maxima strongly depend on β with the rest parameters fixed, in

particular, for $\beta \geq 0.657$ it shows very interesting behavior with further increment in β; both maximum becoming more pronounced and getting more closer accompanied with a shift to higher frequencies. Moreover, the second set of peaks are greater in magnitude than the first set of peaks for n_2, when β is increased like the real part n_1. The large positive value of the imaginary part n_2 of the refractive implies that at the two resonant frequencies there is strong absorption of an electromagnetic wave which propagates through the composite.

Also, note that comparison of Figs. 4.3 and 4.4 show that the values of the resonance peaks for $ZnO@Au$ quantum dots (QDs) are larger than the corresponding peaks of the $ZnO@Cu$ quantum dots (QDs), which is attributed to the small value of the damping constant for Au compared with that of Cu.

Next, we vary the filling factor ξ on the real part of the refractive index, while the volume fraction as well as other parameters remains the same.

B. Refractive index as a function of filling factor, ξ

The graphs of the real part of the refractive index as a function of wavelength for different values of filling factors (ξ) are plotted as shown in Figs. 4.5 and 4.6 for $ZnO@Cu$ and $ZnO@Au$ NPs, respectively. The graphs are obtained by progressively increasing ξ from 0.001 to 0.009 in steps of 0.002. It is observed that the graphs exhibit two set of resonance peaks corresponding to two anomaly dispersion of the systems; the first set resonance peaks are located 510 nm and 480 nm, whereas the second set of resonance peaks are located 736 nm and 704 nm, for the system of $ZnO@Cu$ and $ZnO@Au$ NPs, respectively. In both cases, it is seen that the peaks position remain almost constant (no shift) independent of the values of ξ. Moreover, the peak values increases with an increase of the value of ξ; which suggests that light propagates in the system more readily when concentration (ξ) of the nanoinclusions is small. Thus, as Figs. 4.5 and 4.6 depict, the refractive index near the resonance can

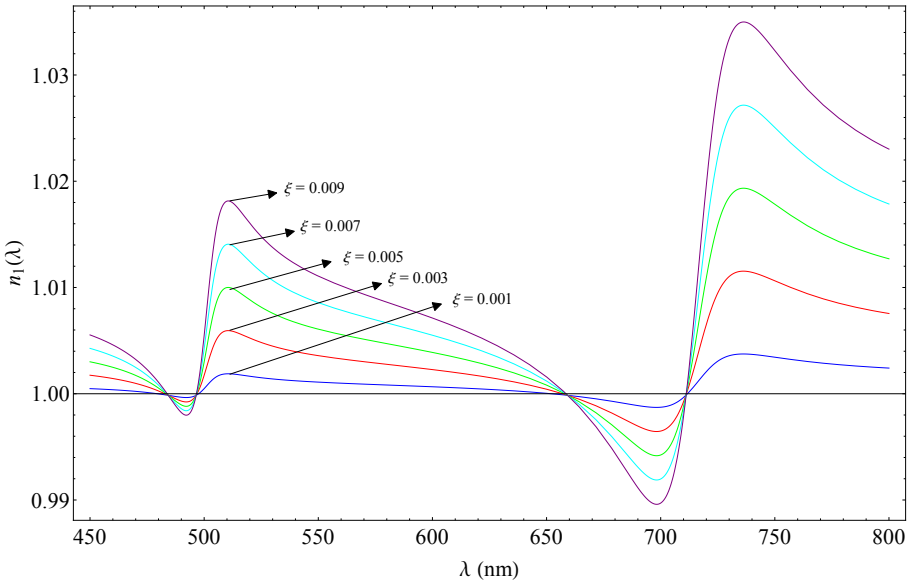

Figure 4.5: The real part of refractive index of $ZnO@Cu$ nanoparticles as a function of wavelength for fixed value of volume fraction β and different values of filling factor ξ.

be tuned by changing the filling factor (ξ), i.e., the density of the packed nanosphere arrays, which can play a great role in applying the core-shell structure in practical applications such as sensors. Similar to that observed in Figs. 4.1 and 4.2, the peak values for $ZnO@Au$ NPs are slightly larger than that of the corresponding peak values for $ZnO@Cu$ NPs because of the small values of the damping constant for Au than Cu.

Figures 4.7 and 4.8 depict the graphs of the imaginary part of the refractive index as a function of the wavelength of the incident radiation for different values of the filling factor (ξ). Similar to Figs. 4.5 and 4.6, for each of the $ZnO@Cu$ and $ZnO@Au$ NPs there are two sets of peaks are located 500 nm and 716 nm for $ZnO@Cu$ NPs; and 477 nm and 689 nm for $ZnO@Au$ NPs) that are attributed to the resonances at the inner core@metal and the outer metal@vacuum interfaces. It is seen that as ξ is increased, the peak values of the resonances also increases; while the peaks positions

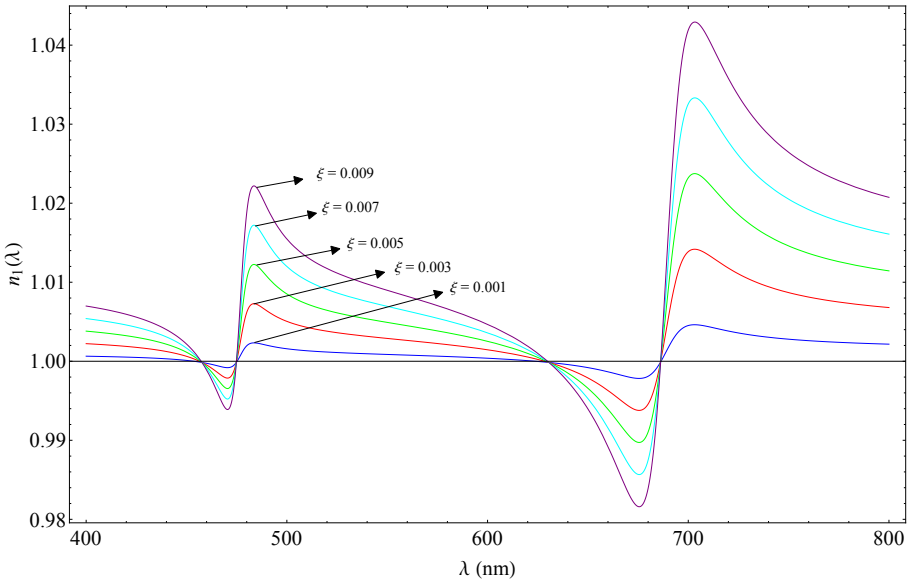

Figure 4.6: The real part of refractive index of $ZnO@Au$ nanoparticles as a function of wavelength for fixed value of volume fraction β and different values of filling factor ξ.

remains constant independent of the value of ξ. It is worth noting that the peaks positions is mainly a function of the electron plasma frequency, ω_p and the size of the nanoparticles. In our case, the size of both the $ZnO@Cu$ and $ZnO@Au$ NPs is fixed at 30 nm and hence the variation in the peaks positions of the two systems is due to solely the difference in the plasma frequency of Cu and Au. Also, the peaks are broader for $ZnO@Cu$ NPs than that of the $ZnO@Au$ NPs which is attributed to the relatively large value of the damping constant of the copper shell.

4.2.2 Optical absorbance

The main optical properties of a semiconductor are typically its refractive index $\tilde{n}$ and absorption coefficient (α) or equivalently the real and imaginary part of the relative permittivity as well as their dispersion relations that depend on the electromagnetic radiation wavelength or photon energy.

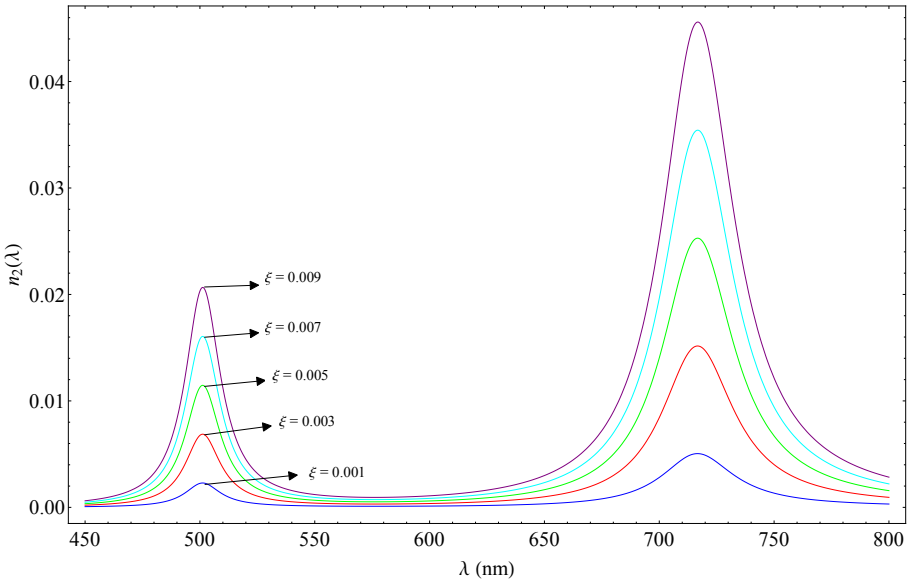

Figure 4.7: The imaginary part of refractive index of $ZnO@Cu$ nanoparticles as a function of wavelength for fixed value of volume fraction β and different values of filling factor ξ.

Consider systems that consists of spherical $ZnO@Cu$ and $ZnO@Au$ core-shell nanocomposites. The spherical nanoparticles in the composites are assumed to be polarized with light-induced dipoles, where the dipole moments interacts with an applied uniform electromagnetic field that is propagates in the $z-$direction is given by;

$$E = E_0 e^{i\omega(n_1 z/c - t)} e^{-\omega n_2 z/c}.$$

It is worth noting that the term $e^{-\omega n_2 z/c}$ implies that the wave decays as it propagates in the core-shell systems [33].

An incident light that propagates in the medium not only is attenuated by absorption but also is involved in a scattering process taking place in the system. However, for nanoparticles that are much smaller than the wavelength of light, scattering effects may be avoided, so that only the absorption contributes significantly to the attenuations. The intensity (I) of the propagating wave is related to the electric field

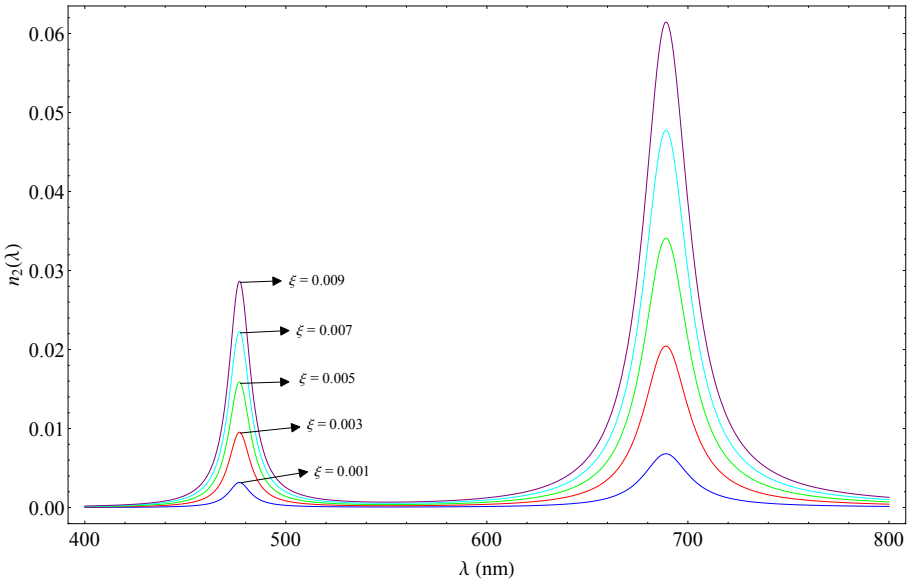

Figure 4.8: The imaginary part of refractive index of $ZnO@Au$ nanoparticles as a function of wavelength for fixed value of volume fraction β and different values of filling factor ξ.

by $I \sim |E|^2$. As the wave transverses the medium the irradiance is exponentially attenuated [31, 32]. That is,

$$I = I_0 \exp^{-\alpha z}, \tag{4.2.6}$$

where I_0 is incident light intensity at $z = 0$ and α is the absorption coefficient defined by;

$$\alpha = \frac{2n_2\omega}{c} = \frac{4\pi n_2}{\lambda}. \tag{4.2.7}$$

Here, $\omega/c = 2\pi/\lambda$ is the frequency of the incident radiation and n_2 is the imaginary part of the refractive index. The typical length of light propagation (or absorption length) l and absorbance $A(\lambda)$ may be calculated from Eq. (4.2.6). We notice that for the coated spherical core-shell nanostructures, the absorption length can be found with the help of $l = 1/\alpha$. From Eq. (4.2.6), we derive the expression for absorbance as $A = \ln I_0/I = t_{s,Cu,Au}\alpha$, where I is the intensity at a thickness $z = t$. Therefore, for

the $ZnO@Cu$ and $ZnO@Au$ nanoparticles the absorbance at metal/shell interfaces is given by;

$$A_{Cu,Au}(\lambda) = \frac{2n_2\omega}{c} t_{s,Cu,Au} = \frac{4\pi n_2}{\lambda} t_{s,Cu,Au}, \tag{4.2.8}$$

where $t_{s,Cu,Au}$=$r_{s,Cu,Au} - r_c$ is the thickness of the copper and gold shells.

C. Absorbance versus shell thickness

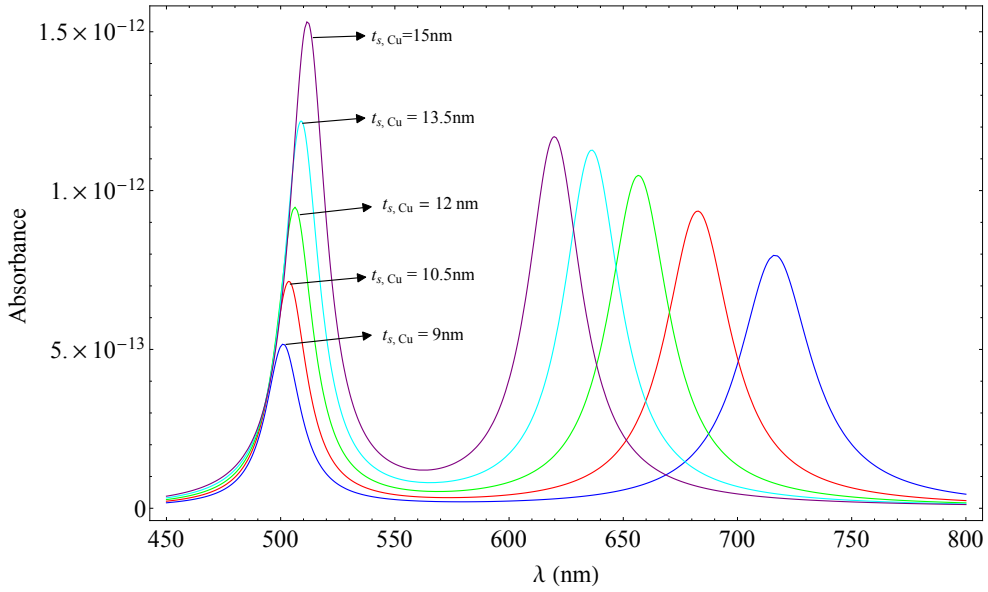

Figure 4.9: The absorbance of the $ZnO@Cu$ nanoinclusions obtain for different values of t_{Cu} and $\xi = 0.001$.

Figures 4.9 and 4.10 display the absorbance spectra of the spherical $ZnO@Cu$ and $ZnO@Au$ nanoinclusions as a function of wavelength for a constant value of ξ and different values of the thickness of the metallic shells $t_{s,Cu,Au}$; with the NPs size fixed constant, i.e., $r_s = 30\ nm$. It shows two sets of absorption peaks are both in the visible spectral region. It observed that when the shell thickness is increased from $9\ nm, 10.5\ nm, 12\ nm, 13.5\ nm$ and $15\ nm$, the first set of resonance peaks attain their maximum values around $510\ nm$ and $490\ nm$ for $ZnO@Cu$ and $ZnO@Au$ NPs,

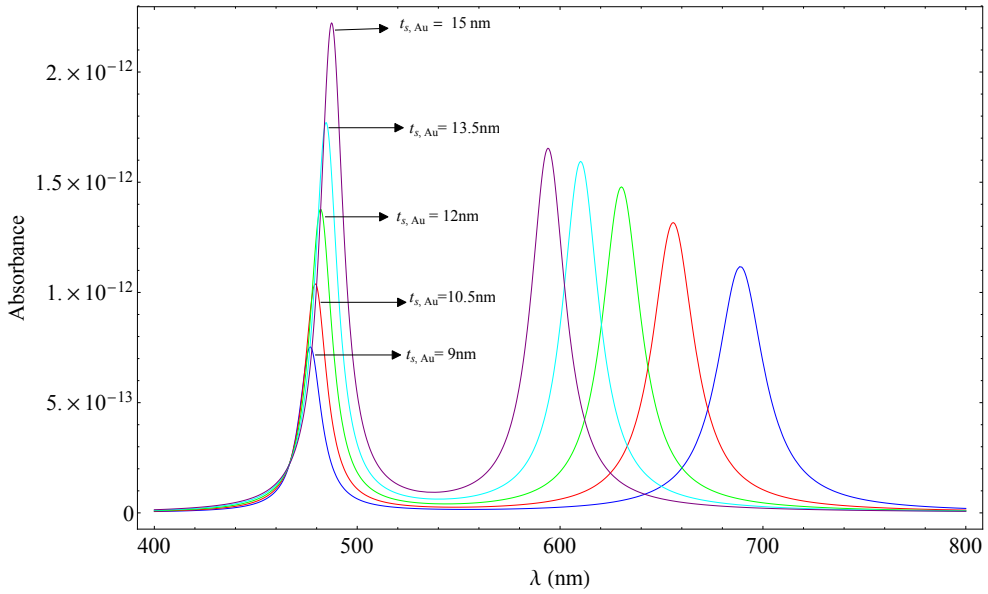

Figure 4.10: The absorbance of $ZnO@Au$ nanoinclusions obtain for different values of t_{Au} and $\xi = 0.001$.

respectively, accompanied with a red shift as the thickness of the shell is increased. These set of resonances may be attributed to the near band edge absorption, due to free exciton recombination. Decreasing the size of the core nanoparticles or increasing the shell thickness moved the absorption edge in the blue spectral regions towards the short wavelength. The shift of the absorption edge is attributed to the change in the energy gap of the nanoparticles. It means that because the band gap of nanostructures semiconductor is increased with decrease in their size called the quantum size effect.

On the other hand, the second set of resonance peaks attain their maximum values around 720 nm and 680 nm for $ZnO@Cu$ and $ZnO@Au$ NPs, respectively. The absorption still increase when the thickness of the shell is increased, but is blue shifted in contrast to that observed for the first set of resonance peaks. These resonance peaks are due to deep level of copper and gold nanoshell. The deep level emission of blue radiation is due to electron recombination in oxygen valance with a hole in the band. The absorption become stronger as the thickness of the copper and gold

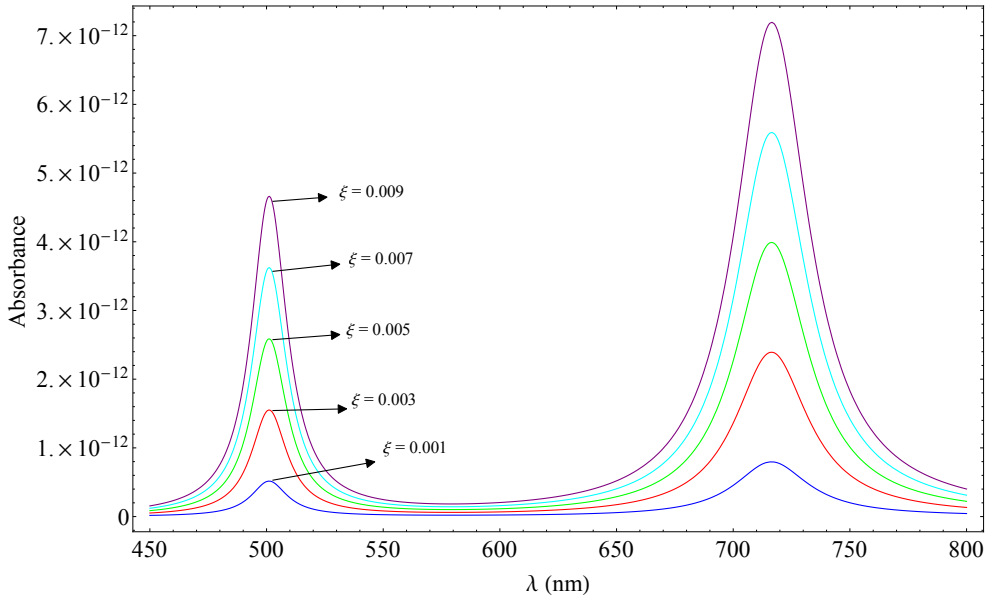

Figure 4.11: The absorbance of the nanoinclusions obtain for different values of ξ to copper the radii of the QDs is $r_s = 30\ nm$.

shell increases from 9 nm, 10.5 nm, 12 nm, 13.5 nm and 15 nm. Furthermore, the optical properties of $ZnO@Cu$ and $ZnO@Au$ nanospheres (ZnO core) are dependent on the nanosphere diameter. Figs. 4.9 and 4.10 show the absorbance spectra for different core diameters such as (21 nm, 19.5 nm, 18 nm, 16.5 nm and 21 nm) with various shell thickness (9 nm, 10.5 nm, 12 nm, 13.5 nm and 15 nm). As core diameter increases, the corresponding peaks split one another at small shell thickness. Short wavelength peak explains resonances on the outer surface of the nanoparticles and long wavelength peaks related by plasmonic resonances on inner semiconductor interfaces. As shell thickness increase both peaks come closer that increase full width at half maximum of efficiency's diagrams [40].

D. Absorbance versus filling factor ξ

Figures 4.11 and 4.12 illustrate the graph of absorbance of a system of spherical core-shell $ZnO@Cu$ and $ZnO@Au$ NPs as a function of the wavelength of the incident

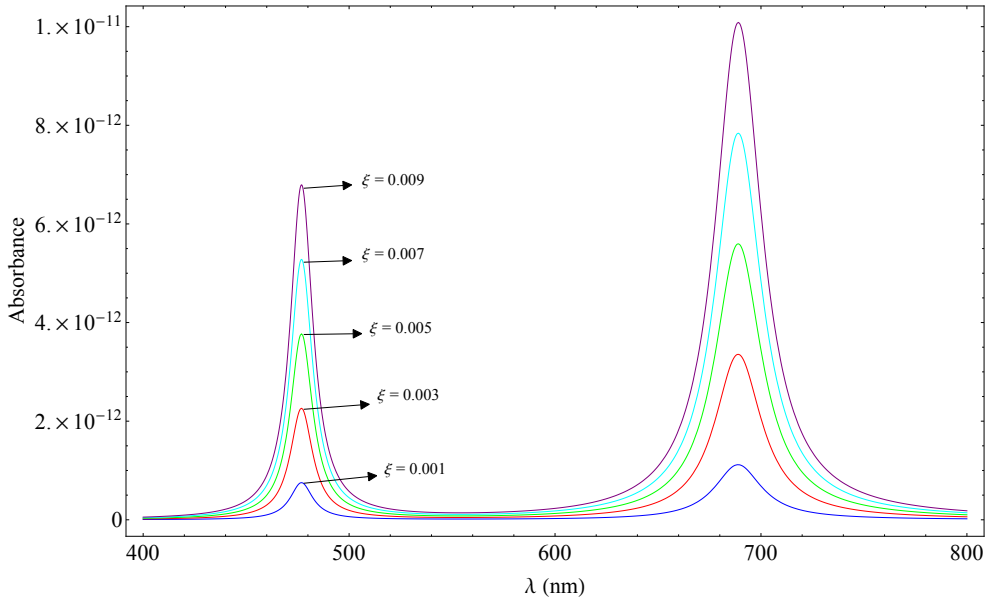

Figure 4.12: The absorbance of the nanoinclusions obtain for different values of ξ to gold the radii of the QDs is $r_s = 30\ nm$.

radiation for different values of filling factor, ξ. The core radii are $r_c = 21\ nm$ and the shell thicknesses are 9 nm. It is observed that the absorbance possess two resonance peaks that progressively increases as ξ increase from 0.001 to 0.009 in steps of 0.002; which suggest that electromagnetic waves (light) is absorbed more in the system when the concentration of the nanoinclusion is large. However, for both systems the peak positions remain almost constant independent of the values ξ, which are located at the wavelengths of 500 nm and 715 nm for $ZnO@Cu$ a system of NPs; and 480 nm and 690 nm for a system $ZnO@Au$ NPs.

Chapter 5

Conclusions

In this work, we studied the effect of varying the core radius and thickness of the metallic shell on the optical response of nanocomposites consisting of spherical $ZnO@Cu$ and $ZnO@Au$ core-shell nanoinclusions embedded in vacuum. The refractive index, and optical absorbance of the system are determined by employing the electrostatic approximation and the Maxwell-Garnett effective medium theory. Moreover, the dielectric function of the copper and gold shell is chosen to be of the modified Drude form that takes into account its nano-size.

It is shown that for different values of the volume fraction β and filling factors ξ, the graphs of the real and imaginary parts of the refractive index of the nanocomposites as a function of wavelength possess two resonance peaks in the visible spectral regions. These resonance peaks correspond to the surface plasmon resonances of at the core@metal shell interface and metallic-shell@host-matrix interface, respectively. The resonance peaks show slight red shift in the low wavelength (blue spectral region) and blue shifts in the high wavelength (red spectral region) when β or $t_{s,Cu,Au}$ is increased. Similarly, for a fixed core-shell radius of 30 nm, the graphs of the optical absorbance versus wavelength for fixed $\xi = 0.001$ and different values of shell thicknesses $t_{s,Cu,Au} = 9\ nm, 10.5\ nm, 12\ nm, 13.5\ nm$ and $15\ nm$) show also two sets of absorption peaks in the same spectral regions. It is observed that when the Cu/Au

shell thickness increases, the two sets of resonance peaks are enhanced; accompanied with slight red shift in the blue and blue shift in the red spectral regions. The enhancement in the optical properties is mainly attributed to strong coupling of the surface plasmon resonance of the Cu/Au shell and the energy gap of the ZnO NPs in both spectral regions. Indeed, compared with the bare ZnO, the copper/gold coated ZnO NPs possess improved potential device applications in the optical frequency region. It is found that the optical properties of spherical $ZnO@Cu$ and $ZnO@Au$ core-shell nanoinclusions embedded in vacuum can be tuned by varying the shell thickness, filling factor, and/or volume fraction of the nanocomposites. The results may be used to optimize 'desired' device parameters of nanocomposites consisting of $ZnO@Cu$ or $ZnO@Au$ core-shell nanostructures that are designed for various applications such as sensors and nano-optoelectronics devices.

Bibliography

[1] Vaidya, Sonalika, Kar, Arik, Patra, Amitava, Ganguli,and Ashok Kumar, *Core–Shell (CS) nanostructures and their application based on magnetic and optical properties*, **Vol. 2, no. 2**, Reviews in Nanoscience and Nanotechnology (2013).

[2] Qi, Weihong, Luo, Linbao, Qian, Hai-Sheng, Ouyang, Gang, Nanda, Karuna Kar, Obare, and Sherine O, *Core-shell nanostructures: modeling, fabrication, properties, and applications*, **Vol. 2012**, Hindawi (2012).

[3] Chaiyachate, Panuwat, Dasri, Thananchai, Chingsungnoen,and Artit, *Theoretical calculation of the optical absorption property of nanoparticles composed of an Au Core and Si shell embedded in silica*, **Vol. 7, no. 1**, Materials Research Express (2020).

[4] Albalwi, Hanan Abdullah, *The Synthesis and Evaluation of Novel Core/Shell Nanoparticles Catalysts*, **Vol. 3, no. 1**, The University of Manchester (United Kingdom) (2016).

[5] Xie, Dini, Peng, Hongshang, Huang, Shihua, You, and Fangtian, *Core-shell structure in doped inorganic nanoparticles: approaches for optimizing luminescence properties*, **Vol. 2013**, Hindawi (2013).

[6] Lee, Gina, *core/shell quantum dots* , **Vol. 10, no. 6282**, Applied science (2020).

[7] Yang, Li-Li, *Synthesis and optical properties of ZnO nanostructures*, Linköping University Electronic Press (2008).

[8] Zhu, Yao, *ZnO nanoparticles as a luminescent down-shifting layer for solar cells*, INSA de Lyon (2015).

[9] Adam, Rania Elhadi, *Synthesis and Characterization of Some Nanostructured Materials for Visible Light-driven Photo Processes*, **Vol. 2059**, Linköping University Electronic Press (2020).

[10] Kelvii Wei Guo, *Property of zinc oxide (Zno) nanostructures potential for biomedical system and its common growth mechanism* , **Vol. 2, no. 5**, Journal of Applied Biotechnology and Bioengineering (2017).

[11] Fleming, Robert *Deformation behavior of Al/a-Si core-shell nanostructures*, University of Arkansas (2017)

[12] Reaz, Mahmud, *Multifunctional Transition Metal Oxide Core Shell Magnetic Nanoparticles*, **Vol. 28, no. 47**, Advanced Materials (2016).

[13] Suresh, Sagadevan, *Semiconductor nanomaterials, methods and applications: a review*, **Vol. 3, no. 3**, Nanosci. Nanotechnol (2013).

[14] Zaini, Muhammad Safwan and Ying Chyi Liew, Josephine and Alang Ahmad, Shahrul Ainliah and Mohmad, Abdul Rahman and Kamarudin, Mazliana Ahmad, *Quantum confinement effect and photoenhancement of photoluminescence of PbS and PbS/MnS quantum dots*, **Vol. 10, no. 18**, Applied Sciences (2020).

[15] Barbagiovanni, Eric G, Lockwood, David J, Simpson, Peter J, Goncharova, and Lyudmila V, *Quantum confinement in Si and Ge nanostructures: Theory and experiment*, **Vol. 1, no. 1** Applied Physics Reviews (2014).

[16] Bera, Debasis and Qian, Lei and Tseng, Teng-Kuan and Holloway, Paul H, *Quantum dots and their multimodal applications: a review*, **Vol. 3, no. 4**, Materials (2010).

[17] Fernandes, Joshua, Kang, and Sangmo, *Numerical Study on the Surface Plasmon Resonance Tunability of Spherical and Non-Spherical Core-Shell Dimer Nanostructures*, **Vol. 11, no. 7** Nanomaterials (2021).

[18] Shweta Bhardwaj, Jim Barr, Elise Chaffin, Xiaohua Huang, and Yongmei Wang, *Near-field and far-field optical properties of magnetic plasmonic core-shell nanoparticles with non-spherical shapes: A discrete dipole approximation study*, **Vol. 5, no. 2** AIP Advances (2019).

[19] Dad Chahinez, Thomas Reji, and Ruedinger Andreas, *Modeling of the surface plasmon resonance tunability of Ag/Au core-shell nanostructures*, **Vol. 8, no. 35**Royal Society of Chemistry (2018).

[20] Alsawafta, Mohammed, *Optical properties of metallic nanoparticles and metallic nanocomposite materials*, Concordia University (2012).

[21] Mendoza Herrera, Luis J and Arboleda, David Munetón and Schinca, Daniel C and Scaffardi, Lucía B, *Determination of plasma frequency, damping constant, and size distribution from the complex dielectric function of noble metal nanoparticles*, **Vol. 116, no. 23**, Journal of Applied Physics (2014).

[22] Jiang, Ruiqian, *Plasmonic nanostructures for surface-enhanced Raman spectroscopy*, The University of Texas at Arlington (2014).

[23] J J Harris, J A Pals and R Woltjer, *Low-Dimensional Structures*, **Vol. 52, no.10**, Materials Science and Engineering: B (2000).

[24] Derkachova, Anastasiya, Kolwas, Krystyna, Demchenko, and Iraida, *Dielectric function for gold in plasmonics applications: size dependence of plasmon resonance frequencies and damping rates for nanospheres*, **Vol. 11, no. 3**, Springer (2016).

[25] Jutika Devi, Rashmi Saikia and Pranayee Datta, *Modeling of absorption and scattering properties of core-shell nanoparticles for application as nanoantenna*

in optical domain, **Vol. 759, no. 1**, Journal of Physics: Conference Series (2016).

[26] Dr. Colton, *Lorentz Oscillator Model* (2020).

[27] Ming Y. Tang, *Modeling and Analysis of Core-Shell Si/SiGe Nanowire*, (2004).

[28] Ahamed, M Irshad, Ahamed, Mansoor and Muthaiyan, R, *Modelling of density of states and energy level of chalcogenide quantum dots*, **Vol. 13, no. 1**, International Review of Applied Sciences and Engineering (2021).

[29] Pan, T, Huang, JP, Li, and ZY, *Optical bistability in metal/dielectric composite with interfacial layer*, **Vol. 301, no. 3-4**, Physica B: Condensed Matter (2001).

[30] Richard D.Averitt, Sarah L.Westcott, and Naomi J.Hanas, *Linear optical properties of gold nanoshells*, **Vol. 16, no. 10**, (1999).

[31] Gashaw Beyene, Teshome Senbeta and Belayneh Mesfin, *Size dependent optical properties of ZnO@Ag core-shell nanostructures*, **Vol. 58**, Chines Journal Of physics (2019).

[32] Jule, Leta T, *Theoretical and experimental study of core-shell structured ZnO/ZnS and growth mechanism of un-doped and doped ZnO nanomaterials*, University of the Free State (Qwaqwa Campus) (2017).

[33] Sisay Shewamare, *Optical properties of metal/dielectric composites with passive and active host matrices*, (2012).

[34] Jhon David Jackson, *classical electrodynamics*

[35] Yilkal Alemu Abbo, *Light waves in a composite of spherical nanoinclusions in passive and active host matrices*, (2014).

[36] V.N.Malnev, Sisay Shewamare, *Slow and fast light in metal/dielectric composition with passive and active host matrices* (2013).

[37] Rocco Citroni, Franco Di Paolo and Aldo Di Carlo, *Replacing noble metals with alternative metals in MID-IR frequency:Atheoretical approach*, Journal of applied physics (2018).

[38] A. V. Mazhukina and O. N. Koroleva, *Calculation of Optical Properties of Aluminum* , **Vol. 2, no. 6**, Institute of Mathematical Modeling, Russian Academy of Sciences, Miusskaya pl. 4A, Moscow, Russia (2010).

[39] Jan Mistrik, Safa Kasap, Harry E. Ruda, Cyril Koughia, Jai Singh , *Optecal properties of electronics materials, Fundamentals and characterizations*, **Vol. 978**, Springer international publshing (2017).

[40] Lysak, Volodymyr V, *Optical properties of core/shell nanoparticles: Comparison of TiO2/Ag and Ag/TiO2 structures*, **Vol. 4**, Materials Today: Proceedings (2017).